Remote Sensing of Environment 251 (2020) 112058

Contents lists available at ScienceDirect

Remote Sensing of Environment

journal homepage: www.elsevier.com/locate/rse

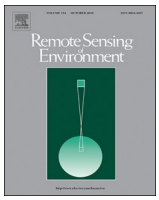

Coral-spawn slicks: Reflectance spectra and detection using optical satellite data

Hiroya Yamano[a,b,*], Asahi Sakuma[a,b], Saki Harii[c]

[a] Center for Environmental Biology and Ecosystem Studies, National Institute for Environmental Studies, 16-2 Onogawa, Tsukuba, Ibaraki 305-8506, Japan
[b] Graduate School of Systems and Information Engineering, University of Tsukuba, 1-1-1 Tennodai, Tsukuba, Ibaraki 305-8577, Japan
[c] Sesoko Station, Tropical Biosphere Research Center, University of the Ryukyus, 3422 Sesoko, Motobu, Okinawa 905-0227, Japan

ARTICLE INFO

Keywords:
Coral mass spawning
Coral bundle
Coral-spawn slick
Satellite constellation
Planet Dove
Sentinel-2

ABSTRACT

This study provides the first report of reflectance spectra of coral-spawn slicks and their detection using optical satellite data. The reflectance spectra show that coral-spawn slicks can be discriminated from other sea-surface features such as wave foam and floating *Sargassum*. Analysis of Planet Dove and Sentinel-2B imagery allowed successful detection of coral-spawn slicks at Ishigaki Island, Okinawa, Japan (24°31′40″N, 124°17′31″E), by using reflectance values in the green and red wavelength regions. This detection was attributable to both their high spatial resolution (3.7 m and 10 m, respectively) and high temporal resolution (1 day and 5 days, respectively), given that coral spawning occurs within a short period (up to several days), typically once a year, and that the coral-spawn slicks have narrow widths of ~10 m. The number of the detected coral-spawn slicks was small, possibly because of coral decline around Ishigaki Island caused by the 2016 worldwide mass coral bleaching event. High-frequency satellite observations, including those from satellite constellations, should provide a powerful tool for understanding coral-reef processes and features whose detection requires high spatial and temporal resolution.

1. Introduction

In marine ecosystems, spawning and larval dispersal play a crucial role in determining the population dynamics, genetic structure, and biogeography of many marine organisms. In terms of conservation, the degree of connectivity between different members of a population is a crucial issue, and this connectivity depends on the dispersal of eggs and larvae. However, as the detection and tracking of eggs and larvae of organisms in the ocean remain challenging, the fate of propagules of these organisms remains unclear.

For reef-building corals, one of the most significant events is the annual synchronized mass spawning (Harrison et al., 1984; Harrison, 2011). By expelling bundles that contain eggs and sperm simultaneously between colonies, the corals increase the likelihood of fertilization. As eggs of many coral species are positively buoyant (Babcock and Heyward, 1986), they commonly accumulate at the sea surface to form coral-spawn slicks (Oliver and Willis, 1987; Willis and Oliver, 1990). Investigation of the generation and fate of the slicks should help to understand the dispersal process of coral larvae and reveal the connectivity of coral reefs.

Remote sensing is the only tool that can reveal the occurrence and extent of coral-spawn slicks and track their movement over wide regions. Oliver and Willis (1987) and Willis and Oliver (1990) visually observed coral-spawn slicks by airplane over a 1000–2100 km^2 area of the Great Barrier Reef of Australia. Those authors observed a total of 59 coral-spawn slicks in three days after a mass spawning event. The slicks ranged from 1 to 10 m in width and from ~15 to 5000 m in length. Although the slicks contained only a small percentage of live embryos (~0.1%, 230 inds m^{-3}) (Oliver and Willis, 1987), it was clear that larval dispersal had occurred. Similar visual observations by airplane have been performed in Okinawa, Japan, for slicks that contained a dense accumulation (~3.6 × 10^6 to ~4.2 × 10^7 inds m^{-3}) of live eggs and embryos (Nadaoka et al., 2002).

Those previous airplane observations encouraged the subsequent observation of coral-spawn slicks using satellite sensors. Thus far, synthetic aperture radar (SAR) data have been used to detect these slicks (Jones et al., 2006; Cresswell et al., 2019), as the slicks exhibit a flat structure that shows specific backscattering features. However, as SAR depends only on surface features, coral-spawn slicks could potentially be confused with other floating materials that exhibit a flat

* Corresponding author at: Center for Environmental Biology and Ecosystem Studies, National Institute for Environmental Studies, 16-2 Onogawa, Tsukuba, Ibaraki 305-8506, Japan.
E-mail address: hyamano@nies.go.jp (H. Yamano).

https://doi.org/10.1016/j.rse.2020.112058
Received 28 April 2020; Received in revised form 23 July 2020; Accepted 24 August 2020

structure (e.g., oil slick) (Brekke and Solberg, 2005). Although coral mass spawning occurs once per year, typically in late spring to early summer (Harrison et al., 1984; Hayashibara et al., 1993), it is possible that other floating materials may be present in the same period. For example, oil spills on the sea surface are seen relatively often (Brekke and Solberg, 2005), floating *Sargassum* may occur during spring and summer in the Caribbean as a result of Amazon River discharge (Wang et al., 2019), and *Trichodesmium* blooms are observed occasionally throughout the year (Westberry and Siegel, 2006).

Examination of both reflectance spectra and satellite data is required to obtain reliable conclusions regarding detection of events (e.g., coral bleaching (Yamano and Tamura, 2004) and occurrence of floating *Sargassum* (Hu et al., 2015)). However, at present, knowledge of both of these is lacking with respect to coral-spawn slicks. No spectral reflectance features are yet available for coral bundles, embryos, and slicks, although spectral libraries for adult coral colonies based on a large number of reflectance measurements have been established (Hochberg et al., 2003; Hochberg et al., 2004; Kutser and Jupp, 2006; Kutser et al., 2006). Furthermore, there have been no reports of successful observation of coral-spawn slicks by optical satellite sensors (Yamano, 2013), although floating *Sargassum* and *Trichodesmium* blooms have been detected and mapped successfully using optical satellite sensors, and routine products are available (e.g., *Sargassum* Watch, https://optics.marine.usf.edu/projects/saws.html).

This difference in detection success may be because of the small areal extent of coral-spawn slicks in comparison with *Sargassum* and *Trichodesmium* blooms. In addition to aerial survey, Willis and Oliver (1990) used Landsat MSS (spatial resolution of 70 m) and SPOT HRV (spatial resolution of 20 m) to assess their feasibility for coral-spawn slick observations. Those instruments allowed detection of oceanographic features such as eddies, wakes, and reflective flat surface water, but slicks were not detected. Willis and Oliver (1990) concluded that the small width of most slicks (3–10 m) compared with satellite image pixel size implied that only very long slicks would be detectable (and only faintly) on satellite images, meaning that such imagery was ineffective for detecting and mapping spawn slicks.

In addition to the limitation imposed by spatial resolution, we argue that insufficient temporal resolution has also inhibited the use of satellite sensors. In particular, the long revisit periods of most satellites make the observation of coral-spawn slicks difficult because the coral mass spawning event occurs over a very short period of up to several days and typically just once a year. Dense cloud coverage in the tropical and subtropical regions obscure observation by optical satellites that have long revisit periods (Hedley et al., 2018).

However, the recent emergence of high-frequency-observation satellites, including satellite constellations, have allowed observations to be made at both high spatial (3–10 m) and high temporal (1–5 day) resolutions. Their application to coral-reef areas is progressing rapidly (Asner et al., 2017; Hedley et al., 2018; Li et al., 2019; Poursanidis et al., 2019; Lyons et al., 2020) and now needs to be extended to study of coral-spawn slicks, which requires observations at high spatial and temporal resolutions. The present study documents the first successful application of optical satellite sensors in detecting and tracking coral-spawn slicks using measurements of spectral reflectance and analysis of Planet Dove (Planet Team, 2017) and Sentinel-2 satellite data.

2. Methods

2.1. Reflectance spectra

Coral bundles with eggs and sperm, their parent colonies, and coral-spawn slicks were collected during a coral spawning event beginning on 3 June 2007 at Akajima Island, Okinawa, Japan (26°11′30″N, 127°16′44″E). A mass coral spawning occurred on 6 June 2007, five days after the full moon. Reflectance spectra of aggregations of bundles of *Acropora* (*Acropora tenuis*, *A. florida*, *A. intermedia*, *A. hyacinthus*, and *A. gemmifera*), *Montipora* (*Montipora* spp.), and *Dipsastraea* (*Dipsastraea* sp. 1 and *Dipsastraea* sp. 2), along with some of their parent colonies (*Acropora tenuis*, *A. florida*, *A. intermedia*, *A. hyacinthus*, and *Dipsastraea* sp. 1 and *Dipsastraea* sp. 2) where available, were measured in a laboratory at Akajima Marine Science Laboratory on Akajima Island. Species of *Acropora* are the dominant corals on Akajima Island (Hayashibara et al., 1993), and their bundles and embryos can form coral-spawn slicks (Nadaoka et al., 2002). In addition to bundles, we measured reflectance spectra of aggregations of the embryos of *A. tenuis* after fertilization to obtain reflectance spectra of coral-spawn slicks composed of embryos. Coral-spawn slicks were observed near Akajima Island after the mass spawning of *Acropora* on 6 June. We collected samples of two coral-spawn slicks and measured their spectra. We also examined the slick samples under a binocular microscope to check whether they were composed of live or dead embryos.

The collected samples, except those of the parent colonies, were set in a cell culture plate, and reflectance spectra were measured at a resolution of 1 nm using a FieldSpec Fr portable spectroradiometer (Analytical Spectral Devices, Boulder, CO, USA), using an attachment that enabled a 5-degree field of view. A halogen lamp (Pro-Light P1–10; Lowel, New York, USA) was used as the light source with ca. 1500 lx and was positioned at a 30° zenith angle approximately 30 cm from the sample. We measured the reflectance of the six parent colonies (*Acropora tenuis*, *A. florida*, *A. intermedia*, *A. hyacinthus*, and *Dipsastraea* sp. 1 and *Dipsastraea* sp. 2) in a flume with black fabric (Yamano et al., 2003) to minimize wall effects in the light field. We measured the upwelling radiance in water from a white reference panel and then from a coral specimen soon after the reference measurement. The spectra were measured about 10 cm above the reference panel and above the corals in order to cover a circle 0.9 cm in diameter, which is within the width of a coral branch. The view zenith angle of the sensor was set to 0 degrees. Four to six samples for each specimen (bundles, embryos, slicks and parent colonies) were measured, and the measurements were repeated 10 times for each sample. Measurements of radiance were expressed as the ratio of the radiance of the sample to that of a reference white panel, and mean reflectance spectra and the standard deviations were calculated. The raw reflectance data and the reflectance spectra (mean and standard deviations) may be found in the Supplementary material (Supplementary Table 1 and Supplementary Fig. 1).

2.2. Satellite data

The recent emergence of high-frequency-observation satellites, including satellite constellations, has allowed observation of coral reefs after mass spawning events of *Acropora*. We obtained Planet Dove and Sentinel-2B satellite images taken at 10:18 and 11:16 (Japan Standard Time, UTC + 9 h) on 18 May 2019, respectively, both of which captured coral-reef areas around Ibaruma, Ishigaki Island, Okinawa, Japan (24°31′40″N, 124°17′31″E) (Fig. 1b). Well-developed fringing reefs, dominated by *Acropora*, are distributed at Ibarauma (Hongo and Kayanne, 2009). The cloud cover during these times was ~30%. At the time of image acquisition, northwesterly winds with speeds of 1.5–2.3 m s^{-1} were recorded at the Ibaruma weather station (AMeDAS, https://www.jma.go.jp/jma/en/Activities/amedas/amedas.html). A newspaper article (https://www.asahi.com/articles/ASM5L3JX0M5LTQIP002.html) and a blog post by an underwater photographer (K. Sekito, https://oceana.ne.jp/from_ocean/93228) reported that a mass spawning event by *Acropora* occurred at Ibaruma at 22:00–22:30 on 17 May 2019.

Table 1 gives the attributes of Planet Dove and Sentinel-2B satellite data used in this study. These satellites differ substantially from the instruments discussed above with respect to their spatial and temporal resolutions. Planet Dove provides imagery using 4-channel, 12-bit multispectral frame cameras in the blue, green, red, and near-infrared (NIR) bands. A critical feature for our work is that Planet Dove provides a daily revisit with a constellation of over 150 satellites. The single-

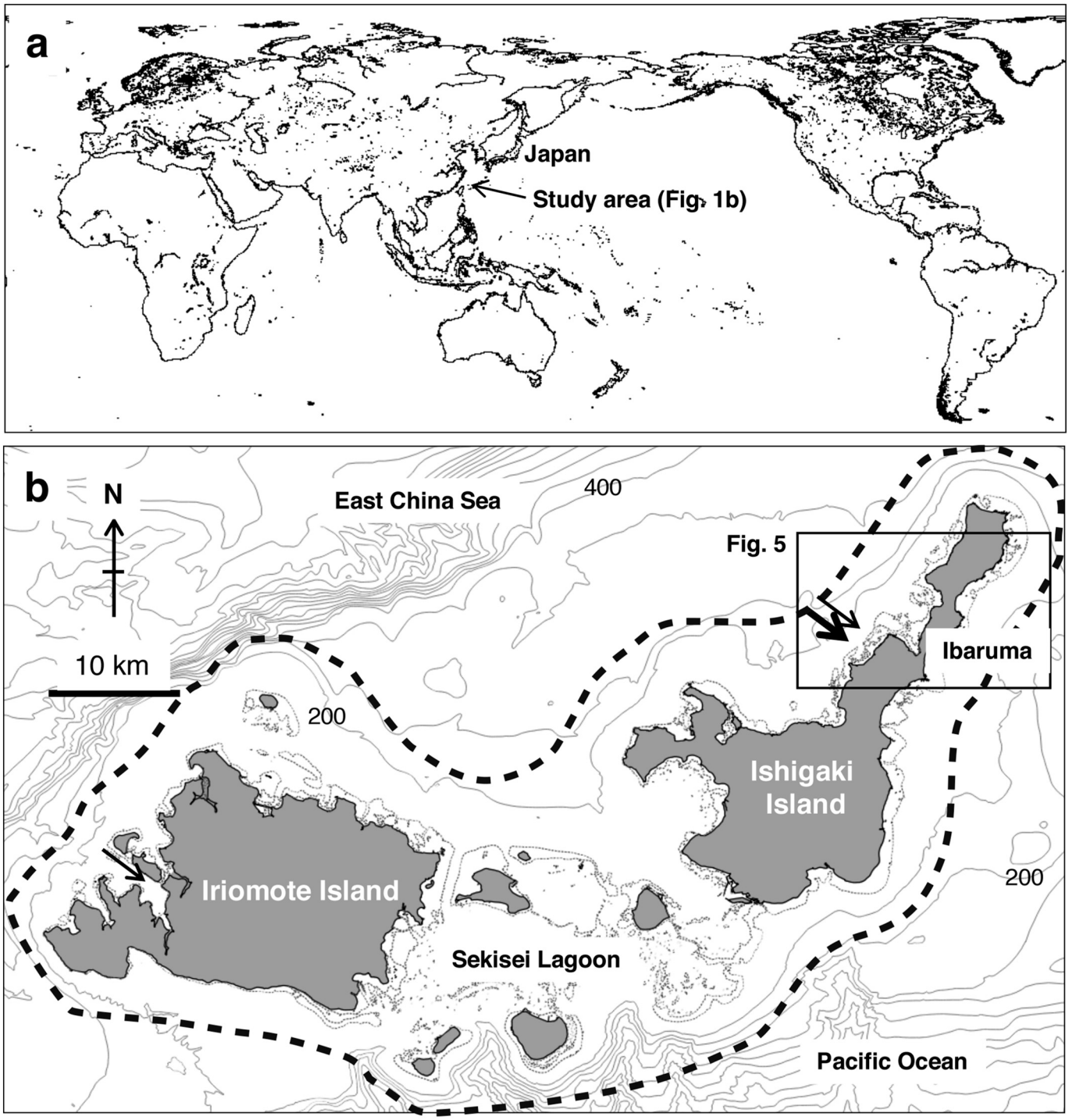

Fig. 1. (a) Location of Ishigaki and Iriomote islands, Okinawa, Japan, showing the study area in which the detection of coral-spawn slicks was investigated. (b) Map of Ishigaki and Iriomote islands. The area of investigation is within the thick dashed line. Numbers indicate water depth in meters. Arrows indicate the locations where coral-spawn slicks were observed. The thick arrow indicates the location of slicks shown in Fig. 5.

scene dimensions are approximately 25 km × 8 km with a spatial resolution of 3.7 m for the four bands. Sentinel-2 provides imagery at several spatial resolutions (10, 20, and 60 m). We used data with 10 m resolution from 4-channel, 12-bit multispectral frame cameras in the blue, green, red, and near-infrared (NIR) bands. Sentinel-2 provides a 5 day revisit interval based on the Sentinel-2A and 2B instrument pair, with a scene width of 290 km. Sentinel-2 data are freely available online (https://registry.opendata.aws/sentinel-2/).

2.3. Image analysis

We used Level 1B and Level 1C data for Planet Dove and Sentinel-2B data, respectively. These data were converted to top-of-atmosphere reflectance by applying the scaling factor supplied with the products. In our Plant Dove data, gaps measuring approximately 10 pixels were observed between the RGB and NIR images. This could be because the RGB and the NIR stripes are two separate acquisitions (approximately 0.5 s apart) (Planet Team, 2016). We thus first performed band re-registration between the RGB and NIR images. Both Planet Dove and

Table 1
Attributes of Planet Dove and Sentinel-2B satellite data used in this study.

Planet Dove			Sentinel-2B		
Band	Wavelength (nm)	Spatial resolution (m)	Band	Wavelength (nm)	Spatial resolution (m)
			1	420–465	60
Blue	455–515	3.7	2	443–541	10
Green	500–590	3.7	3	536–582	10
Red	590–670	3.7	4	646–685	10
			5	694–714	20
			6	730–748	20
			7	766–794	20
NIR	780–860	3.7	8	767–900	10
			8A	848–880	20
			9	930–957	60
			10	1339–1415	60
			11	1540–1681	20
			12	2067–2305	20

Sentinel-2B images were georeferenced with root mean square errors smaller than 0.5 pixels, using a 1:25,000 map for Ishigaki Island published by the Geospatial Information Authority of Japan.

We performed simple dark-pixel atmospheric correction of the images. By assuming that there is a pixel with zero reflectance somewhere in the image, which means that the radiance recorded by the sensor for that pixel is solely from atmospheric scattering, the minimum pixel value was subtracted from those of all other pixels to remove the radiance derived from atmospheric scattering. Pixels from deep ocean areas were used for this correction. We did not perform sun glint correction because no surface glint was observed visually around the coral reefs.

In the visible and NIR wavelength regions able to be observed by Planet Dove and Sentinel-2, the reflectance of coral bundles and coral-spawn slicks showed low values in the blue and green regions, with higher values in the red region and highest in the NIR region (Figs. 2 and 3). On the basis of these characteristics, the red/green band ratio ($RGR = Rr/Gr$, where Rr and Gr are the reflectances of the red and green bands, respectively) was calculated and then used to detect the spatial extent of coral-spawn slicks.

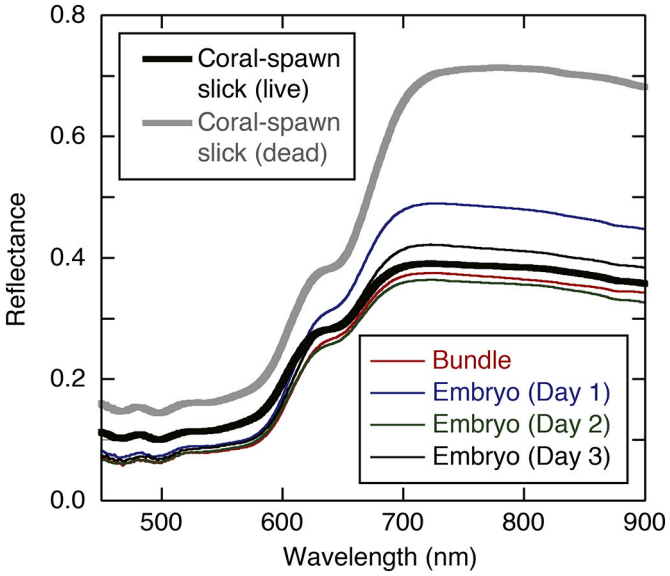

Fig. 3. Reflectance spectra of *Acropora tenuis* bundles and embryos after fertilization, along with those of coral-spawn slicks dominated by live embryos and dead embryos. Reflectance spectra for *A. tenuis* embryos were measured 1, 2, and 3 days after fertilization.

The flight lines of Oliver and Willis (1987) lay 2–5 km off from their studied coasts or coral reefs, and we therefore set a buffer zone of ~5 km from coastlines and coral reefs (Fig. 1b) to investigate coral-spawn slick occurrence. The area, where we searched the slicks, was estimated to be ~1400 km^2, and considering the cloud cover (~30%), the effective area was ~1000 km^2.

3. Results and discussion

3.1. Spectral reflectance features

Fig. 2 shows reflectance spectra of *Acropora*, *Dipsastraea*, and

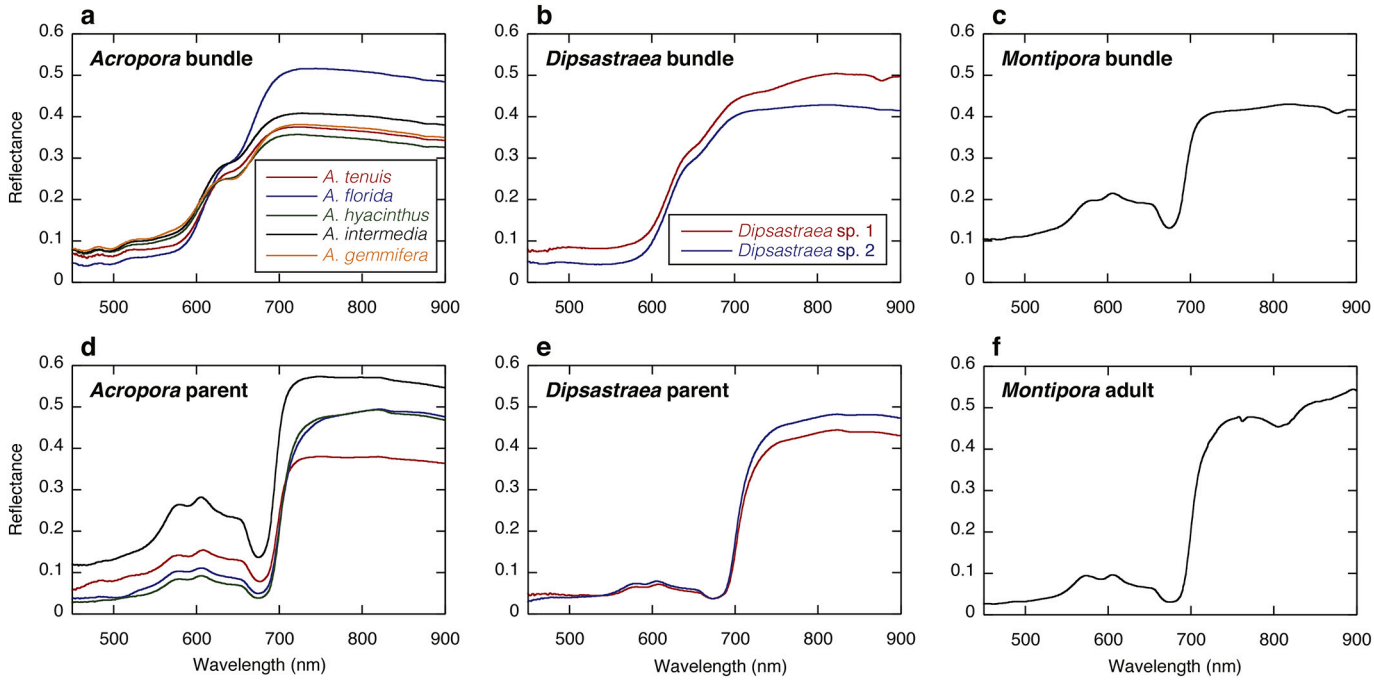

Fig. 2. Reflectance spectra of coral bundles and the parent colonies. *Acropora* (a), *Dipsastraea* (b), and *Montipora* (c) bundles. *Acropora* (d) and *Dipsastraea* (e) parent colonies, and a *Montipora* (f) adult colony. Reflectance spectra of the *Montipora* adult colony (*M. digitata*) are from Yamano et al. (2003).

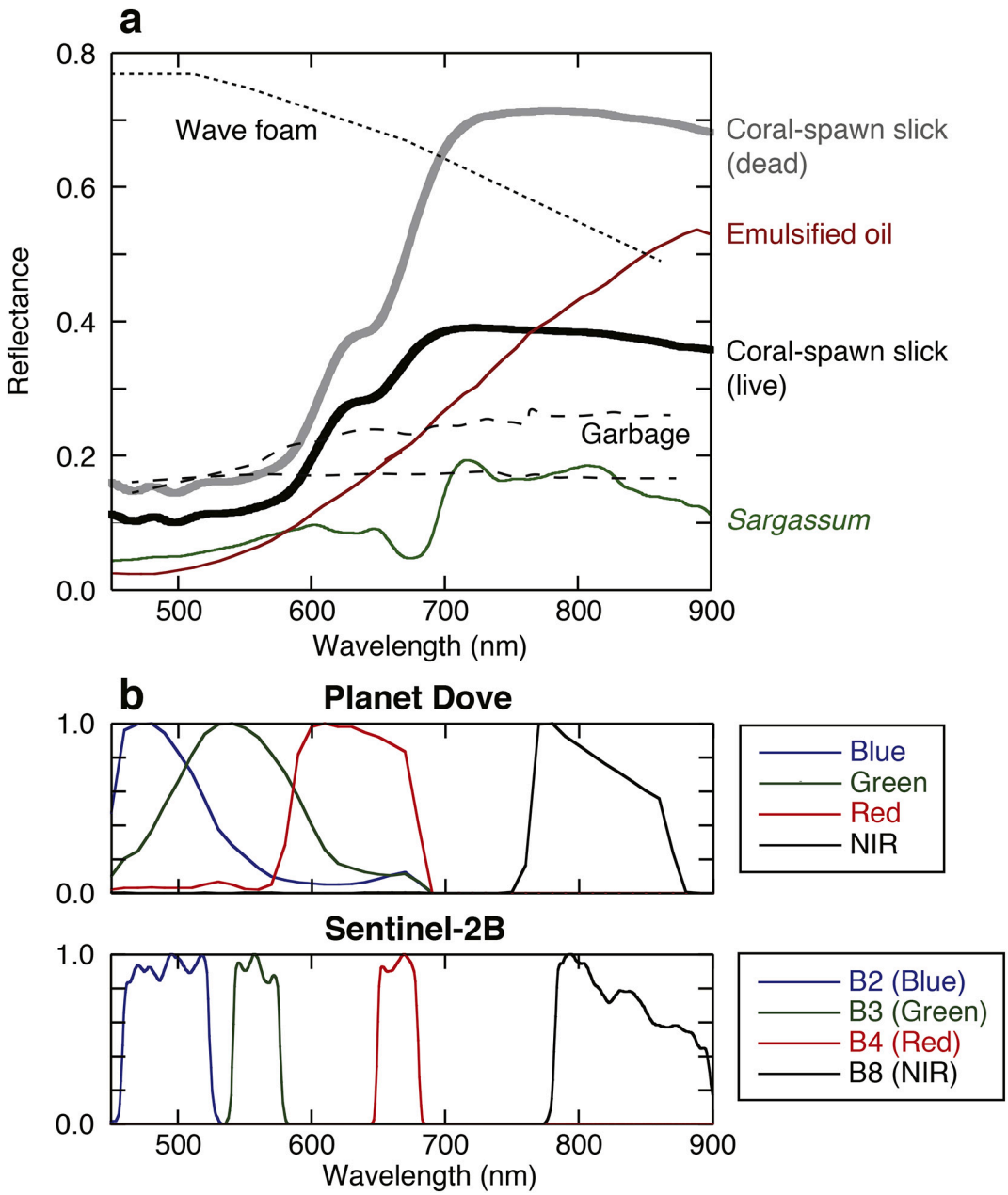

Fig. 4. (a) Reflectance spectra of coral-spawn slicks (Fig. 3), wave foam (Moore et al., 1998), and floating materials (Hu et al., 2015). (b) Sensor spectral response curves for Planet Dove and Sentinel-2B.

Montipora bundles (a–c), along with those of the corresponding parent colonies (d–f). Because the parent colonies of *Montipora* were not sampled in this study, we used the spectral reflectance of an adult colony of *Montipora digitata* measured by Yamano et al. (2003). Reflectance spectra of all colonies exhibit low reflectance in the blue and green regions, and higher reflectance in the NIR region, with an absorption peak at around 680 nm. The spectra show positive reflectance features (i.e., local maxima or shoulders) near 575, 600, and 650 nm (Fig. 2d–f). These features are common to "brown coral", whose reflectance is determined by pigment absorption solely by symbiotic algae (Hochberg et al., 2004).

Acropora and *Dipsastraea* bundles were pink colored, whereas *Montipora* bundles were brown colored because their eggs generally contain symbiotic algae (Hirose et al., 2001). *Acropora* and *Dipsastraea* bundles show substantially different reflectance features from those of the parent colonies in the green to red wavelength region (Fig. 2a, b, d, and e). The reflectance in the red region is much higher than that of the parent colonies and lacks an absorption peak at around 680 nm. Positive reflectance features near 575, 600, and 650 nm, which are common in the parent colonies (Hochberg et al., 2004), are not observed. *Acropora* bundles have a relatively flat shoulder at wavelengths between 620 and 640 nm, but *Dipsastraea* bundles show no such features. *Montipora* bundles exhibit similar reflectance features to those of all the parent/adult colonies, with positive reflectance features near 575, 600, and 650 nm (Fig. 2c and f).

Embryos of *A. tenuis* after fertilization were pink colored, as with the bundles. They also show similar reflectance spectra to those of *A. tenuis* bundles, exhibiting a relatively flat shoulder at wavelengths between 620 and 640 nm (Fig. 3). The two coral-spawn slicks were pink and pale pink in color each. The pink slick was composed mainly of live embryos, whereas the pale-pink slick were dominated by dead embryos. Although the absolute reflectance values are different (lower in the live-dominated slick and higher in the dead-dominated slick), they show similar reflectance characteristics to those of *Acropora* bundles and *A.*

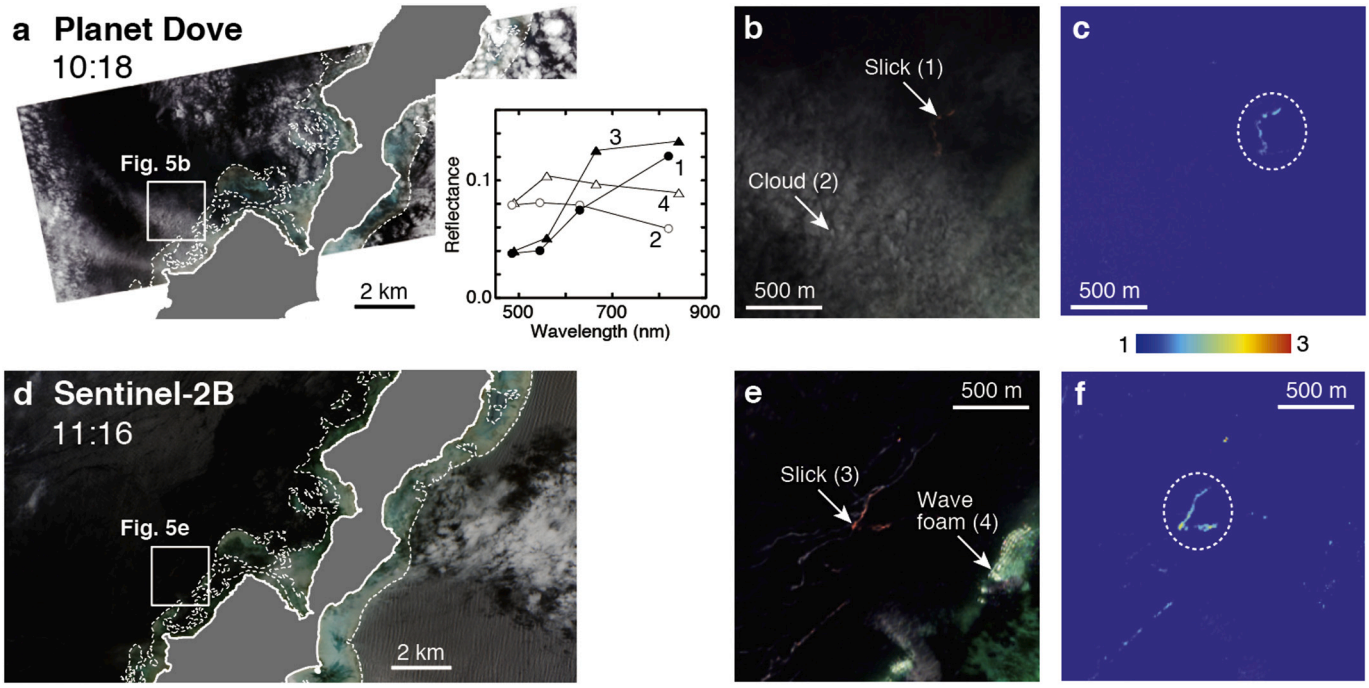

Fig. 5. True-color images for the area around Ibaruma (Ishigaki Island), showing the area with coral-spawn slicks, and the *RGR* values for Planet Dove (a–c) and Sentinel-2B (d–f), respectively. Broken ellipsoids in (c) and (f) indicate main slicks. Image acquisition time (Japan Standard Time) is shown in (a) and (d). Representative examples of the spectral reflectance of coral-spawn slicks, clouds, and wave foam (indicated by arrows) are shown in the inset in (a).

tenuis embryos, with a relatively flat shoulder at wavelengths between 620 and 640 nm (Fig. 3).

Spectral reflectance features of *Acropora*, *Dipsastraea*, and *Montipora* bundles suggest that they can be discriminated by hyperspectral reflectance spectra. The marked spectral difference between *Montipora* bundles and *Acropora* and *Dipsastraea* bundles (Fig. 2a–c) can be explained in terms of the presence/absence of symbiotic algae, which produce spectral features of "brown coral", whose reflectance is determined by pigment absorption solely by symbiotic algae (Hochberg et al., 2004). Among the species examined in this study, only *Montipora* eggs have symbiotic algae (Baird et al., 2009). *Acropora* and *Dipsastraea* bundles can be discriminated using the red wavelength region, whereby *Acropora* bundles have a relatively flat shoulder at wavelengths between 620 and 640 nm (Fig. 2a) and *Dipsastraea* do not (Fig. 2b).

The timing of occurrence of the slicks after the mass spawning of *Acropora* and the similarity of reflectance spectra between coral-spawn slicks and *Acropora* bundles and embryos (Fig. 3) strongly suggest that the coral-spawn slicks were formed mainly by *Acropora*. This supports observations that mass spawning of *Acropora* produces extensive coral-spawn slicks in the wider Indo-Pacific region (Australia: Oliver and Willis, 1987; Philippines: (Jamodiong et al., 2017) and Mozambique: (Sola et al., 2016).

3.2. Distinguishing coral-spawn slicks from other sea-surface features

Coral-spawn slicks could be confused with wave foam and other floating materials, including floating seaweed (e.g., *Sargassum* and *Ulva*), *Trichodesmium* bloom, oil slicks, and garbage. Fig. 4a shows examples of reflectance spectra of wave foam (Moore et al., 1998) and floating materials (Hu et al., 2015), along with those of the studied coral-spawn slicks. Wave foam has high spectral reflectance in the visible wavelength region and decreases with increasing wavelength. *Sargassum*, *Ulva*, and *Trichdesmium* have absorption peaks at ~680 nm on account of the existence of chlorophyll *a*. These characteristics produce lower *RGR* values, allowing discrimination from coral-spawn slicks. Hu et al. (2015) measured *RGR* values of > 1 in *Sargassum*, enabling *Sargassum* to be distinguished from *Ulva* and *Trichdesmium*. Those authors selected narrow wavelengths (647 nm for 1-nm-resolution bands and 645 nm for 10-nm-resolution bands) to obtain positive reflectance features in the red wavelength region. In multispectral bands with wider wavelength regions that include absorption peak wavelengths at ~680 nm, *RGR* values for *Sargassum* should be lower, and discrimination between coral-spawn slicks and *Sargassum* therefore more effective. We calculated surface reflectance values of coral-spawn slicks and *Sargassum* using reflectance spectra and the sensor spectral response curves for Planet Dove and Sentinel-2B (Fig. 4b). Planet Dove, which has a wider red-wavelength region than that of Sentinel-2B, shows *RGR* values of 1.83–1.85 and 1.20 for coral-spawn slicks and *Sargassum*, respectively. The effectiveness of discrimination is better for Sentinel-2B, whose red band is located over the absorption peak in *Sargassum* and which yields higher reflectance values for coral-spawn slicks compared with Planet Dove. *RGR* values of Sentinel-2B are 2.62–2.72 and 0.83 for coral-spawn slicks and *Sargassum*, respectively.

Confusion with oil slicks and garbage should also be considered because both (and particularly oil) show increasing reflectance from blue to NIR wavelength regions, which should give higher *RGR* values (Fig. 4a). In the present study, however, we consider that any confusion between coral-spawn slicks and oil slicks and garbage is unlikely. There is no extensive oil exploitation in the region adjacent to the study area, and garbage should produce lower *RGR* values (Fig. 4a). In addition, garbage is likely to include diverse materials with a range of spectral features (Hu et al., 2015), meaning that *RGR* values of garbage slicks should show a wider range than those of coral-spawn slicks and also be spatially more heterogeneous. We also consider confusion with *Trichodesmium* bloom is unlikely, because *Trichodesmium* blooms occur generally in summer around Japan (Marumo and Asaoka, 1974).

3.3. Detection of coral-spawn slicks using satellite data

Fig. 5a–b, d, and e shows true-color images of Planet Dove and Sentinel-2B images that captured coral-spawn slicks. Satellite-derived reflectance spectra of slicks, along with those of wave foam and clouds,

are displayed in the inset. The coral-spawn slicks exhibit higher reflectance in the red and NIR regions in both Planet Dove and Sentinel-2B images, whereas wave foam and clouds display high and slightly decreasing reflectance from the green to NIR regions. The spectral reflectance features of the slicks in the images agree well with those of coral-spawn slicks (Fig. 4a). The *RGR*, with the lower threshold set to 1, successfully removed most of the wave foam and clouds, allowing coral-spawn slicks to be detected (Fig. 5c and f). *RGR* values of the slicks are higher in the Sentinel-2B image (Fig. 5f) than in the Planet Dove image (Fig. 5c). This can be explained by the difference in wavelength ranges in the red region, as shown by calculating *RGR* values of coral-spawn slicks for Planet Dove (1.83–1.85) and Sentinel-2B (2.62–2.72). As Sentinel-2A has a similar wavelength band assignment to that of Sentinel-2B (Hedley et al., 2018), Sentinel-2 can capture higher spectral reflectance values of coral-spawn slicks in the red wavelength region (Fig. 4) compared with Planet Dove and is thus better suited to their detection.

Although satellite observations have a fundamental limitation imposed by cloudy conditions, compared with SAR, which can penetrate clouds and could detect coral-spawn slicks, data from optical satellites have several advantages over SAR-obtained data (Jones et al., 2006; Cresswell et al., 2019). First, coral-spawn slicks can be discriminated from other floating materials composed of chlorophyll-borne *Sargassum*, *Ulva*, and *Trichodesmium*, which cannot be achieved using SAR, as it observes surface structural features. Second, the detection of coral-spawn slicks using satellites is not affected by weak wind conditions, whereas SAR-based detection of slicks depends critically on wind speed, because wind speeds of < 3 m s^{-1} produce little difference in backscatter between the relatively calm ocean surface, oil slicks, and natural film slicks (Brekke and Solberg, 2005). In the present study, coral-spawn slicks were detected successfully under wind speeds of 1.5–2.3 m s^{-1}.

3.4. Characteristics of coral-spawn slicks

Coral-spawn slicks detected by Planet Dove were ~10–20 m wide and ~500 m long (Fig. 5b). A comparison of Planet Dove and Sentinel-2 images indicates that the main body of the slick was transported ~600 m westward during 1 h. Another slick was detected in the southwestern part of the Sentinel-2B image. However, in the Planet Dove image, it was not possible to judge whether this slick was distinguished because the southwestern part of the image was covered by clouds (Fig. 5a).

The slick widths observed during this study are similar to those observed in the Philippines (Jamodiong et al., 2017) and the Great Barrier Reef of Australia (Oliver and Willis, 1987), but their lengths (~500 m) are shorter than in those studies (~5000 m). Furthermore, we have detected similar-sized slicks in only two other places: to the north of Ibaruma and to the west of Iriomote Island (Fig. 1b), although the dominant coral in this region is *Acropora* (Fujioka, 2001; Hongo and Kayanne, 2009). This means that we observed only a few coral-spawn slicks over an area of ~1000 km^2, whereas Oliver and Willis (1987) observed up to 32 coral-spawn slicks in one day over 1800 km^2.

There are several possible reasons for the occurrence of the short and small number of slicks, including the action of strong winds, which can prevent slick formation, and poorer synchronization of coral spawning (i.e., split over consecutive months or over a few days for different species). However, these possible explanations are unlikely to apply to our study. Rather, we suggest that the spatial resolutions (3.7 and 10 m) used were too coarse to detect narrow slicks < 10 m. Fig. 5e shows that several narrow slicks may be present, but most of them were not detected with the *RGR* (Fig. 5f). Another reason could be the atmospheric correction did not be processed perfectly given the dense cloud condition. Alternatively, the 2016 worldwide mass coral bleaching event (Hughes et al., 2018), which caused a significant decline in corals around Japan, may have led to shorter and small number of slicks. In the Sekisei Lagoon area (Fig. 1b), 85% of the corals were bleached and 5% were dead in July 2016, with 70% of the corals being dead in December 2016 (https://www.env.go.jp/press/files/jp/108072.pdf). *Acropora* was the most affected species, showing 100% bleaching in August 2016 (Nakamura, 2017).

4. Conclusions

By integrating spectral features with satellite data analysis, we have been able to show that coral-spawn slicks can be detected successfully using optical satellite sensors (Planet Dove and Sentinel-2B). This successful detection was made possible by the high spatial resolution (3.7 m and 10 m, respectively) and high temporal resolution (1 day and 5 days, respectively) of these instruments. Constellations of satellites with high spatial resolution are now providing numerous data with high temporal resolution. In response to the suggested applications of high-frequency-observation satellites to understanding the dynamics of coral-reef processes (e.g., bathymetry, bleaching, and sand erosion) (Kutser et al., 2020), our study provides strong evidence regarding the effectiveness of such satellites for detecting a critical aspect of coral-reef functionality requiring high spatial and temporal resolutions; i.e., coral-spawn slicks produced by coral mass spawning.

There are several issues to be examined in applying our results to detect and monitor coral-spawn slicks for other regions. For image processing, in addition to clouds, sun glint is a common confounding factor. Because we performed simple dark-pixel atmospheric correction and did not perform sun glint correction, more sophisticated atmospheric correction and sun glint correction (Kay et al., 2009) may be required. Spectral confusion with other materials (e.g., *Trichodesmium* blooms, oil slicks and garbage) should be examined more in detail, especially for regions where they could co-occur in the coral spawning period. Further, we could expect discrimination of coral-spawn slicks at species/genera level as we showed the difference among *Acropora*, *Dipsastraea* and *Montipora* bundles (Fig. 2), if hyperspectral sensors could be available. Constructing spectral libraries for coral bundles and spawn slicks, in addition to those of the adult colonies, is encouraged, and out raw data (Supplementary Table 1) would contribute to it.

Satellite remote sensing is the only currently available tool that can detect coral-spawn slicks over a wide region. We suggest that this tool should be further applied to tracking coral larvae in order to understand the production and dispersal processes of coral larvae and to reveal the connectivity of coral reefs, by examining the issues presented above. Our results suggest that the short and small number of coral-spawn slicks might have decreased from more usual values because of coral decline caused by the 2016 mass coral bleaching event. This reduction in slick extent and number may lead to delayed recovery of coral reefs. Coral spawning and larval dispersal could be further examined by routine monitoring of coral-spawn slicks using high-frequency-observation satellites.

Supplementary data to this article can be found online at https://doi.org/10.1016/j.rse.2020.112058.

Declaration of Competing Interests

The authors declare that they have no known competing financial interests or personal relationships that could have appeared to influence the work reported in this paper.

Declaration of Competing Interest

None.

Acknowledgments

We thank Akajima Marine Science Laboratory for the use of their facilities. Kenji Iwao, Hironobu Fukami, Go Suzuki, and Masayuki Hatta

provided the coral bundles and allowed us to measure the reflectance of the parent colonies. This paper was improved by the comments and suggestions of three anonymous reviewers.

References

Asner, G.P., Martin, R.E., Mascaro, J., Williams, R., Boyd, D., 2017. Coral reef atoll assessment in the South China Sea using Planet Dove satellites. Remote Sensing Ecol. Conserv. 3, 57–65.

Babcock, R.C., Heyward, A.J., 1986. Larval development of certain gamete-spawning scleractinian corals. Coral Reefs 5, 111–116.

Baird, A.H., Guest, J.R., Willis, B.L., 2009. Systematic and biogeographical patterns in the reproductive biology of scleractinian corals. Annu. Rev. Ecol. Evol. Syst. 40, 551–571.

Brekke, C., Solberg, A.H.S., 2005. Oil spill detection by satellite remote sensing. Remote Sens. Environ. 95, 1–13.

Cresswell, A.K., Tildesley, P.C., Cresswell, G.R., 2019. Synthetic aperture radar scenes of the north west Shelf, Western Australia, suggest this is an underutilised method to remotely study mass coral spawning. J. R. Soc. West. Aust. 102, 45–51.

Fujioka, Y., 2001. Checlikst of hermatypic corals of Urasoko Bay, Ishigaki Island, southserstern Japan. Bull. Nansei Natl. Fish. Res. Inst. 31, 1–11.

Harrison, P.L., 2011. Sexual reproduction of scleractinian corals. In: Coral Reefs: An Ecosystem in Transition, pp. 59–85.

Harrison, P.L., Babcock, R.C., Bull, G.D., Wallace, C.C., Willis, B.L., 1984. Mass spawning in tropical reef corals. Science 223, 1186–1188.

Hayashibara, T., Shimoike, K., Kimura, T., Hosaka, S., Heyward, A., Harrison, P., Kudo, K., Omori, M., 1993. Patterns of coral spawning at Akajima Island, Okinawa, Japan. Mar. Ecol. Prog. Ser. 101, 253–262.

Hedley, J.D., Roelfsema, C., Brando, V., Giardino, C., Kutser, T., Phinn, S., Mumby, P.J., Barrilero, O., Laporte, J., Koetz, B., 2018. Coral reef applications of Sentinel-2: Coverage, characteristics, bathymetry and benthic mapping with comparison to Landsat 8. Remote Sens. Environ. 216, 598–614.

Hirose, M., Kinzie, R.A.I., Hidaka, M., 2001. Timing and process of entry of zooxanthellae into oocytes of hermatypic corals. Coral Reefs 20, 273–280.

Hochberg, E.J., Atkinson, M.J., Andrefouet, S., 2003. Spectral reflectance of coral reef bottom-types worldwide and implications for coral reef remote sensing. Remote Sens. Environ. 85, 159–173.

Hochberg, E.J., Atkinson, M.J., Apprill, A., Andrefouet, S., 2004. Spectral reflectance of coral. Coral Reefs 23, 84–95.

Hongo, C., Kayanne, H., 2009. Holocene coral reef development under windward and leeward locations at Ishigaki Island, Ryukyu Islands, Japan. Sediment. Geol. 214, 62–73.

Hu, C., Feng, L., Hardy, R.F., Hochberg, E.J., 2015. Spectral and spatial requirements of remote measurements of pelagic *Sargassum* macroalgae. Remote Sens. Environ. 167, 229–246.

Hughes, T.P., Anderson, K.D., Connolly, S.R., Heron, S.F., Kerry, J.T., Lough, J.M., Baird, A.H., Baum, J.K., Berumen, M.L., Bridge, T.C., Claar, D.C., Eakin, C.M., GIlmour, J.P., Graham, N.A.J., Hrrison, H., Hobbs, J.-P.A., Hoey, A.S., Hoogenboom, M., Lowe, R.L., McCulloch, M.T., Pandolfi, J.M., Pratchett, M., Schoepf, V., Torda, G., Wilson, S.K., 2018. Spatial and temporal patterns of mass bleaching of corals in the Anthropocene. Science 359, 80–83.

Jamodiong, E.A., Maboloc, E.A., Leriorato, J.C., Tañedo, M.C.S., Diaz, L.A., Tabalanza, T.D., Cabaitan, P.C., Villanueva, R.D., 2017. Coral spawning and spawn-slick observation in the Philippines. Mar. Biodivers. 48, 2187–2192.

Jones, A.T., Thankappan, M., Logan, G.A., Kennard, J.M., Smith, C.J., Williams, A.K., Lawrence, G.M., 2006. Coral spawn and bathymetric slicks in Aynthetic Aperture Radar (SAR) data from the Timor Sea, north-west Australia. Int. J. Remote Sens. 27, 2063–2069.

Kay, S., Hedley, J., Lavender, S., 2009. Sun glint correction of high and low spatial resolution images of aquatic scenes: A review of methods for visible and near-infrared wavelengths. Remote Sens. 1, 697–730.

Kutser, T., Jupp, D.L.B., 2006. On the possibility of mapping living corals to the species level based on their optical signatures. Estuar. Coast. Shelf Sci. 69, 607–614.

Kutser, T., Miller, I., Jupp, D.L.B., 2006. Mapping coral reef benthic substrates using hyperspectral space-borne images and spectral libraries. Estuar. Coast. Shelf Sci. 70, 449–460.

Kutser, T., Hedley, J., Giardino, C., Roelfsema, C., Brando, V.E., 2020. Remote sensing of shallow waters – A 50 year retrospective and future directions. Remote Sens. Environ. 240, 111619.

Li, J., Schill, S.R., Knapp, D.E., Asner, G.P., 2019. Object-based mapping of coral reef habitats using Planet Dove satellites. Remote Sens. 11, 1445.

Lyons, M.B., Roelfsema, C.M., Kennedy, E.V., Kovacs, E.M., Borrego-Acevedo, R., Markey, K., Roe, M., Yuwono, D.M., Harris, D.L., Phinn, S.R., Asner, G.P., Li, J., Knapp, D.E., Fabina, N.S., Larsen, K., Traganos, D., Murray, N.J., 2020. Mapping the world's coral reefs using a global multiscale earth observation framework. Remote Sensing Ecol. Conserv. https://doi.org/10.1002/rse2.157.

Marumo, R., Asaoka, O., 1974. *Trichodesmium* in the East China Sea. J. Oceanogr. Soc. Jpn. 30, 298–303.

Moore, K.D., Voss, K.J., Gordon, H.R., 1998. Spectral reflectance of whitecaps: Instrumentation, calibration, and performance in coastal waters. J. Atmos. Ocean. Technol. 15, 496–509.

Nadaoka, K., Harii, S., Ikema, T., Paringit, E., Mitsui, J., Tamura, H., Iwao, K., Kakuma, S., 2002. Observation of coral spawning and the dynamics of the slicks at Kerama Islands, Okinawa. Proc. Coastal Eng. JSCE 49, 1176–1180.

Nakamura, T., 2017. Mass coral bleaching event in Sekisei lagoon observed in the summer of 2016. J. Jpn. Coral Reef Soc. 19, 29–40.

Oliver, J.K., Willis, B.L., 1987. Coral-spawn slicks in the Great Barrier Reef: Preliminary observations. Mar. Biol. 94, 521–529.

Planet Team, 2016. In: Planet Labs Inc. (Ed.), Planet Imagery Product Specification: PlanectScope & RapidEye. Planet Com, San Francisco, pp. 52.

Planet Team, 2017. Planet application program interface. In: Space for Life on Earth. Planet Com, San Francisco.

Poursanidis, D., Traganos, D., Reinartz, P., Chrysoulakis, N., 2019. On the use of Sentinel-2 for coastal habitat mapping and satellite-derived bathymetry estimation using downscaled coastal aerosol band. Int. J. Appl. Earth Obs. Geoinf. 80, 58–70.

Sola, E., Marques da Silva, I., Glassom, D., 2016. Reproductive synchrony in a diverse *Acropora* assemblage, Vamizi Island, Mozambique. Mar. Ecol. 37, 1373–1385.

Wang, M., Hu, C., Barnes, B.B., Mitchum, G., Lapointe, B., Montoya, J.P., 2019. The great Atlantic *Sargassum* belt. Science 365, 83–87.

Westberry, T.K., Siegel, D.A., 2006. Spatial and temporal distribution of *Trichodesmium* blooms in the world's oceans. Global Biogeochem. Cycles 20, GB4016.

Willis, B.L., Oliver, J.K., 1990. Direct tracking of coral larvae: implications for dispersal studies of planktonic larvae in topographically complex environments. Ophelia 32, 145–162.

Yamano, H., 2013. Multispectral applications. In: Goodman, J.A., Purkis, S.J., Phinn, S.R. (Eds.), Coral Reef Remote Sensing. Springer, Dordreht, pp. 51–78.

Yamano, H., Tamura, M., 2004. Detection limits of coral reef bleaching by satellite remote sensing: Simulation and data analysis. Remote Sens. Environ. 90, 86–103.

Yamano, H., Tamura, M., Kunii, Y., Hidaka, M., 2003. Spectral reflectance as a potential tool for detecting stressed corals. Galaxea, JCRS 5, 1–10.